Vacuum 204 (2022) 111383

Contents lists available at ScienceDirect

Vacuum

journal homepage: www.elsevier.com/locate/vacuum

Application of positive pulse to extract ions from HiPIMS ionization region

Liuhe Li [a,*], Jiabin Gu [a,b], Yi Xu [c,d], Mingyue Han [a], Marcela Milena Marie Bilek [e,f]

[a] Department of Material Processing and Control Engineering, School of Mechanical Engineering and Automation, Beihang University, Beijing, 100191, People's Republic of China
[b] School of Mechanical, Electronic and Control Engineering, Beijing Jiaotong University, Beijing, 100044, People's Republic of China
[c] Institute of Mechanics, Chinese Academy of Sciences, Beijing, 100190, People's Republic of China
[d] Center of Materials Science and Optoelectronics Engineering, University of Chinese Academy of Sciences, Beijing, 100049, People's Republic of China
[e] School of Physics, University of Sydney, Sydney, NSW, 2006, Australia
[f] School of Biomedical Engineering, The University of Sydney, Sydney, NSW, 2006, Australia

ARTICLE INFO

Keywords:
High power impulse magnetron sputtering (HiPIMS)
Ions extraction method
PIC-MCC simulation
Microscopic mechanism of ions extraction

ABSTRACT

High power impulse magnetron sputtering (HiPIMS) is a promising physical vapor deposition technique with one of the main drawbacks being its relatively low deposition rate. In this article, a method was propose by using a positive ions extraction pulse ($U_{extract}$) which would be immediately applied to the sputtering target after the HiPIMS negative pulse to extract out the ions from the ionization region near the HiPIMS target. The Particle-In-Cell/Monte Carlo Collision (PIC-MCC) simulation, experiments, and theoretical study were conducted to investigate the ions extraction process. It is demonstrated that the higher potential moved from the target area to the substrate direction and the peak ion density was driven to the substrate direction, after applying the positive ions extraction pulse to the target. The measured ion-energy distribution function (IEDF) characteristics verified that the ions extraction method works. The experimental results indicated that the Ti^{+} ion flux dramatically increased when the $U_{extract}$ was over 50 V. Good agreement between the experimental and simulation results was obtained, validating the simulation conclusion. Finally, the microscopic mechanism of ions extraction is proposed.

1. Introduction

As one of the most successful methods to increase ionization the degree of sputtered species, high power impulse magnetron sputtering (HiPIMS) has been the focus of research in the field of physical vapor deposition over the last years [1]. It has found widespread application in many industrial sectors due to its significant advantages, such as the high ionization flux fraction (about 78% for Al [2], 70% for Cu [3], 68% for Ti [2], 40% for TiAl [4], 30% for Cr [5]), ultra-dense plasmas with electron density (the order of 10^{18}–10^{19} m^{-3}) [6–9], and high average ion energy [10,11]. However, as deeper as the researches proceed, one shortcoming of HiPIMS technology is exposed. When the process parameters and average power are comparable, the deposition rate of HiPIMS is generally lower than that of conventional DC magnetron sputtering [12–14]. For examples, Helmersson et al. [15] indicated that when the same average power is used, the deposition rate of Cr, Al, Ta, and Zr films synthesized by HiPIMS is only 29%, 35%, 22%, and 15%, respectively, of DCMS. Davis et al. [16] observed that the deposition rate of TiO_2 film sputtered from the Ti target by HiPIMS is 4–7 times lower than that of DCMS. Ma et al. [17] also suggested that the deposition rate of TiAlSiN coatings sputtered from the TiAlSi target by HiPIMS is about 88% of DCMS using the constant average power.

1.1. Optimizing HiPIMS plasma sources through power supply and magnetic field

The low deposition rate problem has led researchers to reconsider the merits of HiPIMS technology. Many researchers, either theoretically or technologically, have been paying attention to the physical mechanism of this issue. Until now, the most widely accepted explanation of this problem is that the high negative pulse target voltage takes part in a double-edged sword role in the HiPIMS, as follows: the secondary electrons generated by the Ar^{+} bombardment in front of the target could gain enough energy from the cathode sheath to promote the ionization of the sputtered particles. However, it is extremely difficult for these ions to escape from the ionization region in the target vicinity, as a result of

* Corresponding author.
E-mail address: liliuhe@buaa.edu.cn (L. Li).

https://doi.org/10.1016/j.vacuum.2022.111383
Received 26 March 2022; Received in revised form 25 July 2022; Accepted 27 July 2022
Available online 1 August 2022

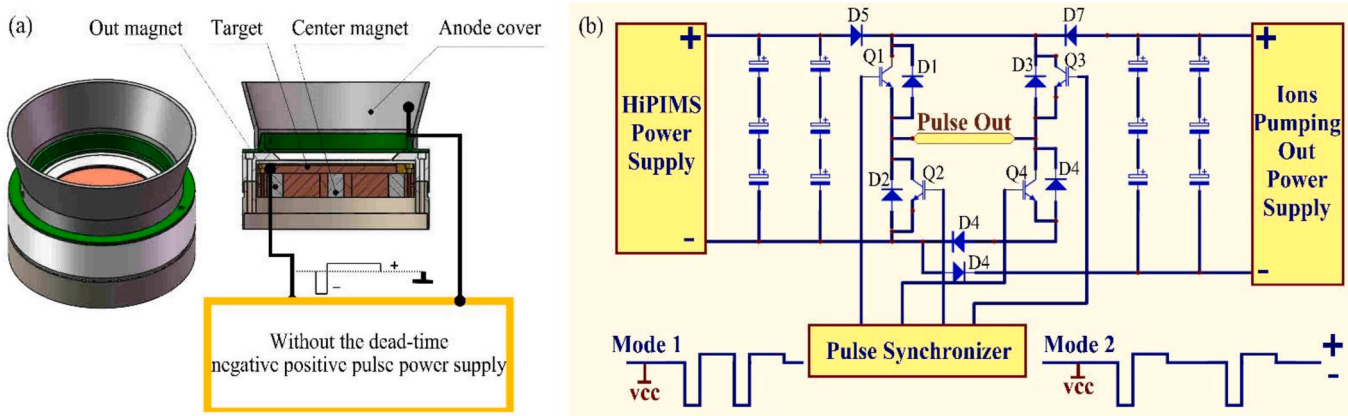

Fig. 1. Ion extraction method to increase deposition rate, (a) schematic diagram of the initial program, (b) circuit diagram of the program.

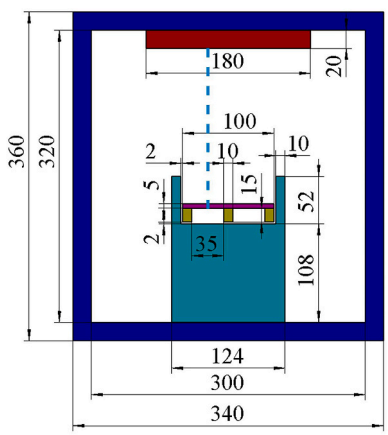

Fig. 2. The cross-section of the PIC-MCC modeled simulation geometry representing a cylindrical vacuum chamber with a circular magnetron and substrate holder. The unit of the dimension is mm.

Table 1
Other parameters of the PIC-MCC calculation.

Items			Value	Unit
Grid			1 × 1	mm
Original plasma temperature			8	eV
Original ions and electrons density			4.0	10^{14} m^{-3}
Number of electrons/ions per super-particle			10^8	–
Base pressure			0.4	Pa
The electron time step (t_{step})			4	10^{-11}s
The 1st period	Negative pulse voltage: U_{HiPIMS}		−800	V
	Negative pulse width		2.3	μs
The 2nd period	1	Positive pulse voltage: $U_{extract}$	800	V
		Positive pulse width	48	ns
		Substrate bias	−100	V
	2	Positive pulse voltage: $U_{extract}$	400	V
		Positive pulse width	0.2	μs
		Substrate bias	0	V

back attraction or the returning ion effect [18–20]. The ions that reached to the downstream substrate are most likely in a diffusion mechanism [21]. To increase the ions flux towards downstream, as well as the deposition rate, lots of approaches and means has been proposed. In terms of power supply, the modulated pulsed power (MPP) magnetron sputtering has been developed [22–24] and the deposition rate of MPP even exceeds the deposition rate of DCMS when preparing Cr and Al coatings [25,26]. Pulse drive technology in which HiPIMS is superimposed with DC [27,28] or mid-frequency (MF) [29,30] has also been proposed that the deposition rate can be effectively increased. Lattemann et al. [31] found that the deposition rate of DLC coatings in the mixed HiPIMS and arc mode is 8 times higher than that of the conventional HiPIMS. In terms of magnetic field optimization, Mishra et al. [32] reported the deposition rate of the Ti coatings was increased by a factor of 6 through a small reduction in the magnetic field strength (33% at the target). Other studies have also reported that the deposition rates of Nb [33] and V coatings [34] prepared by HiPIMS have increased by a factor of 5 and 2.6, respectively, by reducing the magnetic field strength. McLain et al. [35] found that by using the linear tripack magnet pack the deposition rates of Cu coatings prepared by HiPIMS could be equal to or greater than that of DC with a standard magnet pack. Li et al. [36] observed that in the case of HiPIMS assisted by the external electric field and external magnetic field simultaneously, the deposition rates were approximately 73% higher compared to the conventional HIPIMS.

1.2. Method for extracting ions using positive pulses

For optimizing the power supply to increase the deposition rate, in addition to the MPP and HiPIMS together with the DC and MF voltage approaches, applying a reverse positive voltage right after the primary HiPIMS negative pulse may improve the deposited ion flux, as suggested by Konstantinidis et al. [37] early. Later, Nakano et al. [38] found that the plasma density could be increased by applying a positive target bias voltage during the pulse-off period. From 2013, Li [39,40] also proposed a method by using an auxiliary electric field, that is, a positive pulse, which is used to extract out the ions from HiPIMS ionization region, would be immediately applied to the sputtering target after the negative HiPIMS pulse (Fig. 1). The positive pulse can be applied not only to the sputtering target, but also to the anode cover, or to both the sputtering target and the anode cover. The application of the anode cover can optimize the ion diffusion and a detailed description can be found in our earlier works [39,41]. To avoid the ions which may have had a velocity to the target during the HiPIMS pulse, the transition time between the negative HiPIMS pulse and the positive extraction pulse should be as short as possible. This method is different from another approach suggested by Nakano et al. [38,42], in which a positive potential is applied to the sputtering target after the negative HiPIMS pulses to raise the plasma potential and in this way to accelerate ions towards the growing film. By considering that a DC or pulse-off positive voltage exerted on the target can only increase the plasma potential in the whole chamber, its effect would have not much difference with a more negative substrate bias. In addition, a DC or pulse-off positive voltage may accelerate lots of ions to bombard the vacuum chamber and lead to iron contamination, possibly. In Li's scheme, a positive pulse mode is proposed instead of DC or pulse-off positive voltage mode, so that the plasma in the chamber has

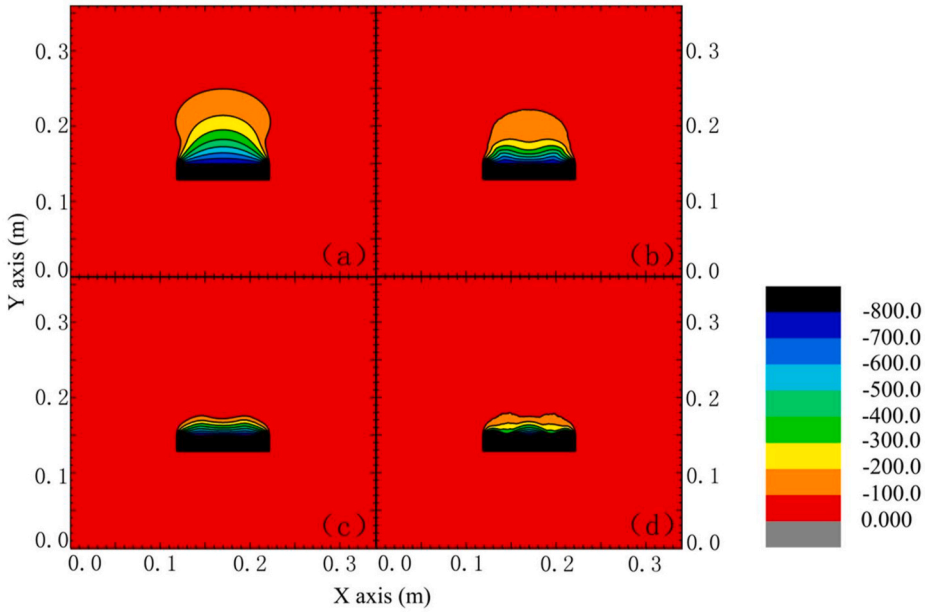

Fig. 3. The potential distribution in the model at different times. (a) $t = 0$ s, (b) $t = 2 \times 10^{-8}$ s, (c) $t = 1.2 \times 10^{-6}$ s, (d) $t = 2.3 \times 10^{-6}$ s.

enough time to lower its potential to the ground to facilitate ion extraction in pulsed mode. With this intention, the related design of power supply (as shown in Fig. 1(b)), theoretical plasma dynamics research based on Particle-In-Cell/Monte Carlo (PIC-MCC) were carried out, when applied to the National Natural Science Foundation of China in 2016 [39,40]. Then the relevant confirmatory experimental research were completed in Helmersson's lab at Linköping University. In fact, the ions extraction method has been published by some other researchers [43–52]. This method was named bipolar pulsed HiPIMS. The advantages of using this method (such as increasing deposition rates [43], controlling ion energy [46–50], improving film properties [51,52], etc.) have been discussed in previous studies. Despite numerous studies showing the benefits of this HiPIMS modification, in the ions extraction method, the details of particle motion and evolution, the invitation motive, and the microscopic mechanism of ions extraction are still lacking.

In this work, the ion extraction method has a distinct feature that distinguishes it from other bipolar pulsed magnetron sputtering: the ion extraction positive pulse width is much wider than the HiPIMS's negative one so that the ions have enough time to be driven to the substrate. This work is organized as follows. The details of our simulation and experimental setup were described in Section 2. In section 3, the simulation result of the ions extracts out method was presented. The simulation is by using a PIC-MCC method which is based on Kwok's code [53,54] and developed by Luo [55] by integrating Vahedi's method [56]. The HiPIMS discharge process and ion extraction process were simulated by the PIC-MCC method. After the positive pulse was applied to the target, the evolution of plasma potential, ion velocity and position, and ion density were simulated and calculated. Section 4 presents the experimental results and discussion. In this section, the voltage and current waveforms of the discharge, the ion energy distribution function (IEDF), and the integrated intensity of the ion flux were explored. By comparing the simulation results with the experimental results, the microscopic mechanism of ion extraction is finally proposed finally.

2. Simulation and experimental setup

2.1. Simulation details

In this work, the PIC-MCC method [55] is used to simulate the transport of atoms sputtered from the target in the presence of Ar background gas. The PIC-MCC method is developed and described in Ref. [55]. The simulation geometry is presented in Fig. 2 and its dimensions were provided in Fig. 2 as well. It comprises as follows:

(i) A cylindrical discharge chamber (blue color, outer dimension Φ340 mm × 360 mm, the thickness is 20 mm).
(ii) A circular target holder (Cyan color, Φ124 mm × (108 + 52) mm) in the center of the chamber. The upper side of the holder is a cylinder chimney with a height of 52 mm.
(iii) A target (pink color) is located in the bottom and center of the chimney with a diameter of Φ100 mm × 5 mm.
(iv) A cylinder magnetic bar and a cylinder magnetic ring are beneath the target (yellow color, height is 15 mm) and is 2 mm away from the target holder.
(v) A circular substrate holder (red color, Φ180 mm × 20 mm) is placed inside the chamber at a target-to-substrate distance of 190 mm, the working pressure is assumed as 0.4 Pa.
(vi) The gas inlet and outlet are neglected.

Because the simulation is so time-consuming process and to avoid the error accumulations, the following simplified assumptions in the simulation are used.

- Only one species of inert gas Ar is used in the simulation. That is, if the Ar^+ bombed the titanium target, the sputtered out atoms are still Ar atoms, so that the parameters such as the elastic collision cross-sections remain unchanged. Because such assumptions can avoid continuous judgment of species and frequent changes in the relevant simulation parameters. It is reasonable because this assumption did not affect the qualitative analysis of whether the ions are extracted out. We only focus on the movement dynamics of the ions cloud driven by the positive pulse within the ionization reign.
- It is reasonable to assume that neutral excited states of Ar have the same elastic collision cross-sections as the ground states. In the first approximation, the density of Ar in this work can be regarded as the sum of all neutral Ar under the base pressure. Of course, the introduction of ionization and other processes would create reaction pathways that are different for ground and excited states.

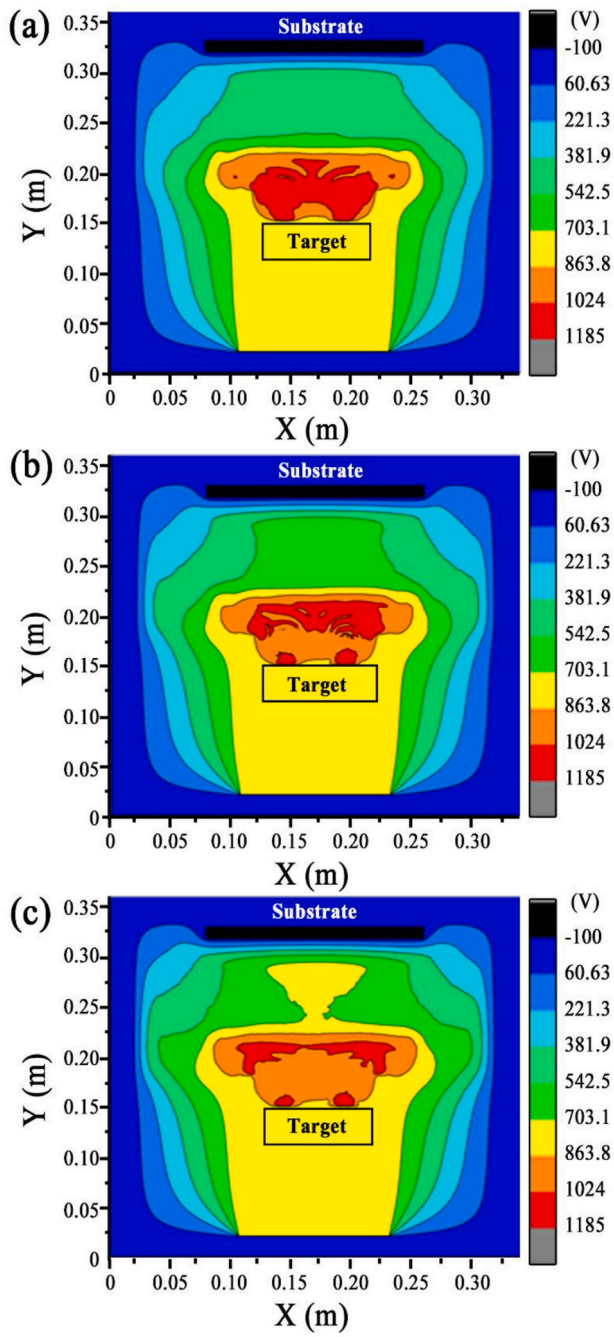

Fig. 4. The potential distribution of an "extract pulse" applied to the target at the end of the 2.3 μs HiPIMS "sputter pulse", (a) $t = 0 \times t_{step}$, (b) $t = 600 \times t_{step}$, (c) $t = 1200 \times t_{step}$, time step $t_{step} = 4x10^{-11}$s.

- When the Ar^{+} species sputter the target, the secondary electrons would also be generated if the energy of Ar^{+} is over the secondary emission threshold. The secondary electrons emission current is according to the secondary electron yield of the target, which is a linear fit of the secondary electron yield as a function of ion velocity in this study [57]. The generated electron original velocity is assumed as 0 at the beginning of the pulse.
- PIC-MCC simulation is used to simulate the HiPIMS plasmas and its self-developed discharges. However, it is too complicated for the collisions if all the possible collisions are considered. So in this work, the collisions between ions and neutral species, and electrons and ions are all neglected. Only the collisions between electrons and neutral species are adopted. That is, $e + Ar \rightarrow e + Ar$, $e + Ar \rightarrow e + Ar^{*}$ and $e + Ar \rightarrow e + Ar^{+} + e$ are taken into account.
- To build up the collisions for the PIC-MCC simulation, an original thin plasma with a density of $4.0 \times 10^{14}/m^{3}$ was distributed evenly in the simulation chamber (Fig. 2), which has been measured in the normal HiPIMS discharge [58]. The sputtering pressure is 0.4 Pa, so the original ionization rate is in the 10^{-6} order and it is little enough and would not affect the simulation results. Other parameters of the PIC-MCC calculation were listed in Table 1.

The simulation was divided into two periods. The 1st period is to simulate the HiPIMS discharge. In the 1st period, the negative pulse voltage of −800 V with a width of 2.3 μs is applied to the target. The 2nd period is to simulate the ions extraction procedure. In the 2nd period, two different positive voltages of 800 V and 400 V were respectively applied. The 800 V one is used to accelerate the electric field dynamic change process. The 400 V one is to show the ions dynamic movement tendency. By PIC-MCC simulation of the positive pulse applied to the target immediately after the negative HiPIMS pulse, the plasma potential, ions velocities and positions, and ions density can be calculated for different simulation times. It should be noted that only a very short time of the positive pulse was used because as the calculation proceeding, the particle propagated rapidly so that the calculation process becomes too time-consuming.

2.2. Experimental details

The experiments' detailed setup has been described in the reference [49]. A Φ220 mm × 300 mm cylindrical chamber was equipped with the titanium sputtering magnetron target in the center of it. The target is 50 mm in diameter and is mounted facing upward. The cathode is connected to a pulsing unit which is fed with negative, and ions extracting out positive pulse potentials as programmed by a synchronization unit (a HiPSTER prototype from Ionautics AB). The vacuum chamber was evacuated to a base of $\sim 10^{-7}$ Torr ($\sim 10^{-5}$ Pa) for the sputtering discharge. During sputtering an Ar flow (99.997% purity) of 50 sccm and an N_2 flow (99.995% purity) of 0.35 sccm are used. The total pressure is maintained at 0.66 Pa using a throttle valve. A PSM003 mass spectrometer (Hiden Analytical Ltd) capable of measuring ion energies up to 100 eV is used for measuring the ion-energy distribution function (IEDF) of Ar^{+}, Ar^{2+}, Ti^{+}, Ti^{2+}, N^{+}, and N_2^{+}. The sampling orifice, which is aligned with the center of the Ti target at a distance of ~8 cm, has an opening of 300 μm in diameter and is grounded during the measurements. The energy step size is set to 0.1 eV while the acquisition per data point is set to 200 ms corresponding to 140 pulses averaged per data point. During the acquisition of the IEDF presented in this work the positive ions extraction voltage ($U_{extract}$) were set to 0, 10, 25, 50, 75, 100, and 150 V. The discharge current and voltage are recorded by Tektronix TDS 2004C. The negative pulse (the conventional HiPIMS pulse) has a length of 30 μs and is operated at a repetition frequency of 700 Hz.

3. Simulation results and discussions

3.1. The 1st period PIC-MCC simulation

The 1st period is to simulate the HiPIMS discharge to obtain the ions and electrons distributions parameters for the 2nd period.

Fig. 3 shows the potential distribution at the first 2.3 μs of HiPIMS discharge. From Fig. 3(a)–(d), it can be seen that the potential contour lines were pushed to the target surface which is corresponding to the HiPIMS sheath building up procedure, and this is consistent with many HiPIMS discharge researches [59,60]. From Fig. 3(c) and (d), it can also be concluded that above the racetrack region where the magnetic lines are parallel to the target surface, the plasma potential was changed more rapidly than other upper areas of the target. After 2.3 μs discharge, the

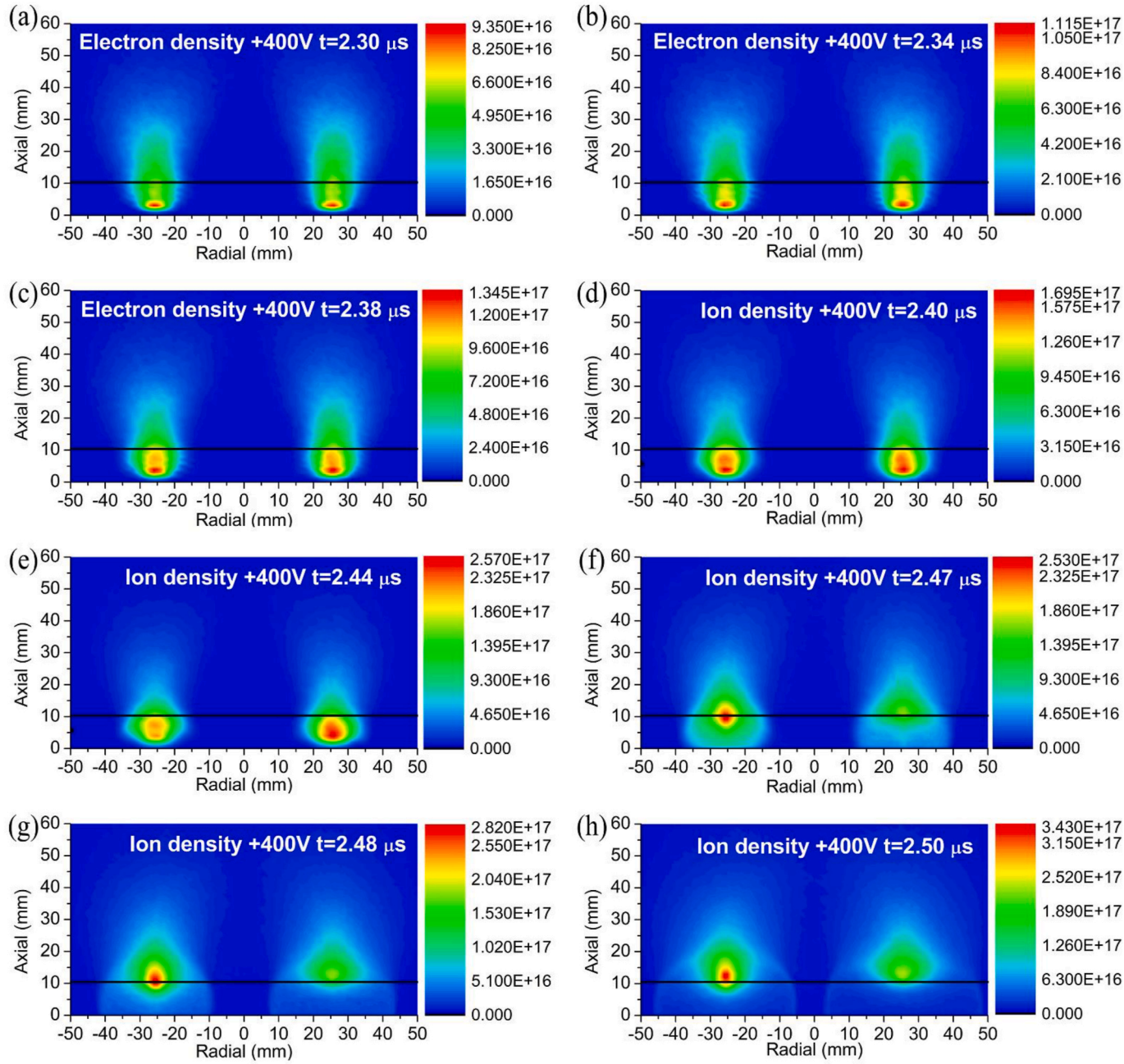

Fig. 5. The ions density distribution at the time of (a) $t = 2.30$ μs (the time $U_{extract}$ are used), (b) $t = 2.34$ μs, (c) $t = 2.38$ μs, (d) $t = 2.40$ μs, (e) $t = 2.44$ μs, (f) $t = 2.47$ μs, (g) $t = 2.48$ μs, (h) $t = 2.50$ μs.

ions have accumulated to the upper area of the sputtering trace. The densities of electrons and ions have reached the order of 10^{17} m^{-3} at this time. For the HiPIMS discharge, the plasma density is generally in the order of 10^{17} m^{-3}, which brings many challenges for a computer to simulate a large discharge domain. In the present work, the negative pulse duration (1st period) was set at 2.3 μs when the plasma density just exceeds to 1×10^{17} m^{-3}. This timescale is long enough to generate a HiPIMS plasma, as claimed in both experimental measurement [58] and simulation [59]. With the increase of ions and electrons, the calculation speed would be decreased rapidly. So the simulation with the negative voltage of −800 V was ended at 2.3 μs. All the data obtained in the 1st period simulation, such as the ion density, electrons density, super-particles positions, and velocities, are all reserved and as initial parameters for the 2nd period positive pulse calculation.

3.2. The 2nd period PIC-MCC simulation

Electric field characteristics when a positive pulse $U_{extract}$ was applied to the target would determine whether the extract pulse takes effect or not. So, in the 2nd period simulation, two different simulations were taken up. (1) The $U_{extract} = 800$ V was calculated for 48 ns to speed up the potential field's variation. (2) The $U_{extract} = 400$ V was to show the movement of the ions. The calculated results of the 1st period were used as the initial parameters of the 2nd period calculation, which signifies that the positive pulse was applied to the target immediately after the negative pulse without the dead-time.

3.2.1. Electric field characteristics with $U_{extract} = 800$ V

The potential distribution results are shown in Fig. 4. The results at time $t = 2.3$ μs meant that meant the calculation had finished the first

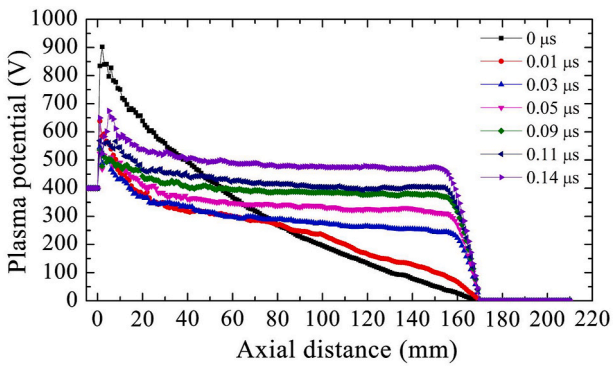

Fig. 6. Calculated results of temporal and axial distribution of the plasma potential above the racetrack (shown in dot line in Fig. 2).

calculation step and at the same time the target had a positive potential of 800 V. The ion density, electrons density, and super-particles positions were still not changed, only the electric field was recalculated because the target voltage had changed from −800 V to +800 V. It can be seen that the highest potential area is not 800 V at the target. The highest potential area is located at the upper space of the racetrack (the ionization region, in red color). The positive potential reached as high as 1185 V. This should be due to the distribution of ions and electrons which was obtained in the last calculation period. This is also evidence that the ions cloud should have been formed at the end of the negative pulse and that there is still a plasma sheath. It should be noted that only a short time of 2.3 μs calculation was carried out to simulate the HiPIMS discharge. The plasma sheath must be still in a dynamic state since the ions density only reached to near the order of 10^{17} m^{-3}. So the high potential area (in red color in Fig. 4(a)) is between $y = 0.13$ m (the position of the target surface) and $y = 0.18$ m, which is much thicker than the statistic plasma sheath.

From Fig. 4, it can be obviously seen that the higher potential moved from the target area to the substrate direction. At the $t = 600 \times t_{step} = 0.024$ μs (Fig. 4(b)), the highest potential reached to $y = 200$ mm (0.20 m) area. While at $t = 1200 \times t_{step}$ (Fig. 4(c)), it reached to 220 mm.

Not only the highest potential which is corresponded to ions distribution moved to the substrate, but the potential between the target with the substrate and even the potential in the whole chamber also increased too. This indicates that the electrons are attracted by the target when the ions are repelled.

3.2.2. *Ions distribution character when $U_{extract} = 400$ V*

Fig. 5 shows the calculation results of ion density distribution between $t = 2.3$ μs and $t = 2.5$ μs. During this period, the $U_{extract}$ was a positive one with a value of 400 V. Horizontal dotted lines were drawn to compare the changes in the peak position of ions density at different times. It can be clearly seen that the peak ion density (red color) was driven to the substrate direction slowly. At the same time, the value of the peak ion density would still keep increasing from 9.500×10^{16} m^{-3} to 3.430×10^{17} m^{-3}. This denotes that further ionization was appeared by using the following positive extraction voltage.

3.2.3. *Temporal evolution of plasma potential when $U_{extract} = 400$ V*

Fig. 6 is the temporal and spatial evolution of the plasma potential calculated after the $U_{extract}$ (+400 V) is exerted. They are the calculated results at the axial direction, along the dotted line shown in Fig. 2, and the plasma potential plotted at different delay times. From Fig. 6 it can be found, just at the beginning (time = 0+), there would be a high voltage which is higher than the $U_{extract}$ and less than $U = U_{extract} - U_{HiPIMS}$. This can be explained by considering that the ion sheath still has a higher net ion density in front of the target at the end of the HiPIMS negative pulse and the "overshoot" phenomenon. The "overshoot" phenomenon is caused by the strong magnetic field in front of the target blocking the movement of the electron flow towards the target [61]. It is also coincided with Velicu's experimental results [62] from two points. Firstly, at the earlier time, near the target, there would be a high potential plasma. Second, as the time elapsed, the collapse of the sheath and the downstream movement of ions lead to an increase in the plasma potential far away from the target. This corresponds to the phenomenon that the peak of ion density (red) in Fig. 5 is slowly driven to the direction of the substrate. One difference is that the potential increasing speed and double layer structure of the plasma are not so obvious. This can be explained by the fact that the parameters, such as the width of the HiPIMS pulse and the magnetic field used, in our calculation are different from theirs. We believed that higher potential near the target is the motivity of the ions to be extracted out.

4. Experimental results and discussions

Fig. 7 shows the discharge voltage (Fig. 7(a)) and current (Fig. 7(b)) pulse waves applied to the target with and without the following extraction voltage pulses $U_{extract}$ ($U_{extract} = 0$ V, 10 V, 50 V, 100 V or 150 V, $U = 0$ V is marked as R-HiPIMS), respectively. A discharge current wave ($U_{extract} = 0$ V) in the dashed line was also shown in Fig. 7(a), to sign the discharge current and voltage synchronization. The HiPIMS negative pulse width was 30 μs and the following ions extraction positive pulse width was 200 μs with a dead time of about 2 μs at a repetition frequency of 700 Hz.

From Fig. 7(b) it can be found that the HiPIMS discharge current amplitude could be affected by the following extraction positive pulse. Without the extraction pulse, the maximum HiPIMS discharge current is −13.5 A. While it increased with the increasing of the extraction pulse voltage and reached to 16.3 A when the extraction pulse is 150 V (see zoom in I in Fig. 7(b)). This indicated that the extraction positive voltage applied to the target could increase the electric conductivity of the HiPIMS system at a repetition frequency of 700 Hz. The positive $U_{extract}$ would attract electrons to the region near the target surface. However, these electrons were trapped into the archy magnetic field above the target surface and would keep the inspiral-like movement and vibrating near the target. This may increase the ionization of the background gas and Ti atoms, leading to an increase in the discharge current. Thus, the extraction pulse increased the plasma disappearance time and higher positive voltage makes the conductivity of the rare background gas in the chamber better.

Fig. 7(b) shows not only the negative HiPIMS current pulse but also the positive current during the extraction positive pulse applied to the target. In Fig. 7(b), the zoom in II picture shows the detail of the positive current at the beginning of the $U_{extract}$ pulse. It can be seen that at all extraction pulse cases, the positive current with the maximum magnitude of 0.6 A was much higher than that of the R-HiPIMS one in which no extraction pulse was used. The maximum positive current was only about 0.06 A in the R-HiPIMS case. The increase in positive current may be due to additional heating or reverse discharge of electrons [63,64], which is consistent with the simulation results of an increase in peak ion density (Fig. 5). Similar results have also been reported in Refs. [44,46,64] where the positive currents were observed during positive pulses of bipolar HiPIMS discharges.

The IEDF of Ar^+, Ti^+, and, N^+ ion species gained by the PSM003 ion mass spectrometer were shown in Fig. 8.Fig. 8(a)–(f) show the IEDF of Ar^+, Ti^+, and N^+ ion species, respectively. It should be noted that the PSM003 ion mass spectrometer can only measure the ion energies up to 100 eV. So all the IEDF curves are the section within +100 eV. The IEDF curves for HiPIMS with $U_{extract}$ have a number of characteristic features similar to Ref. [46] that has been detailedly described by Ulf Helmersson, where the nitrogen was not fed. For the $U_{extract} = 100$ V and 150 V, the IEDF only showed the first 100 eV section.

The typical characters of the IEDF are as follows:

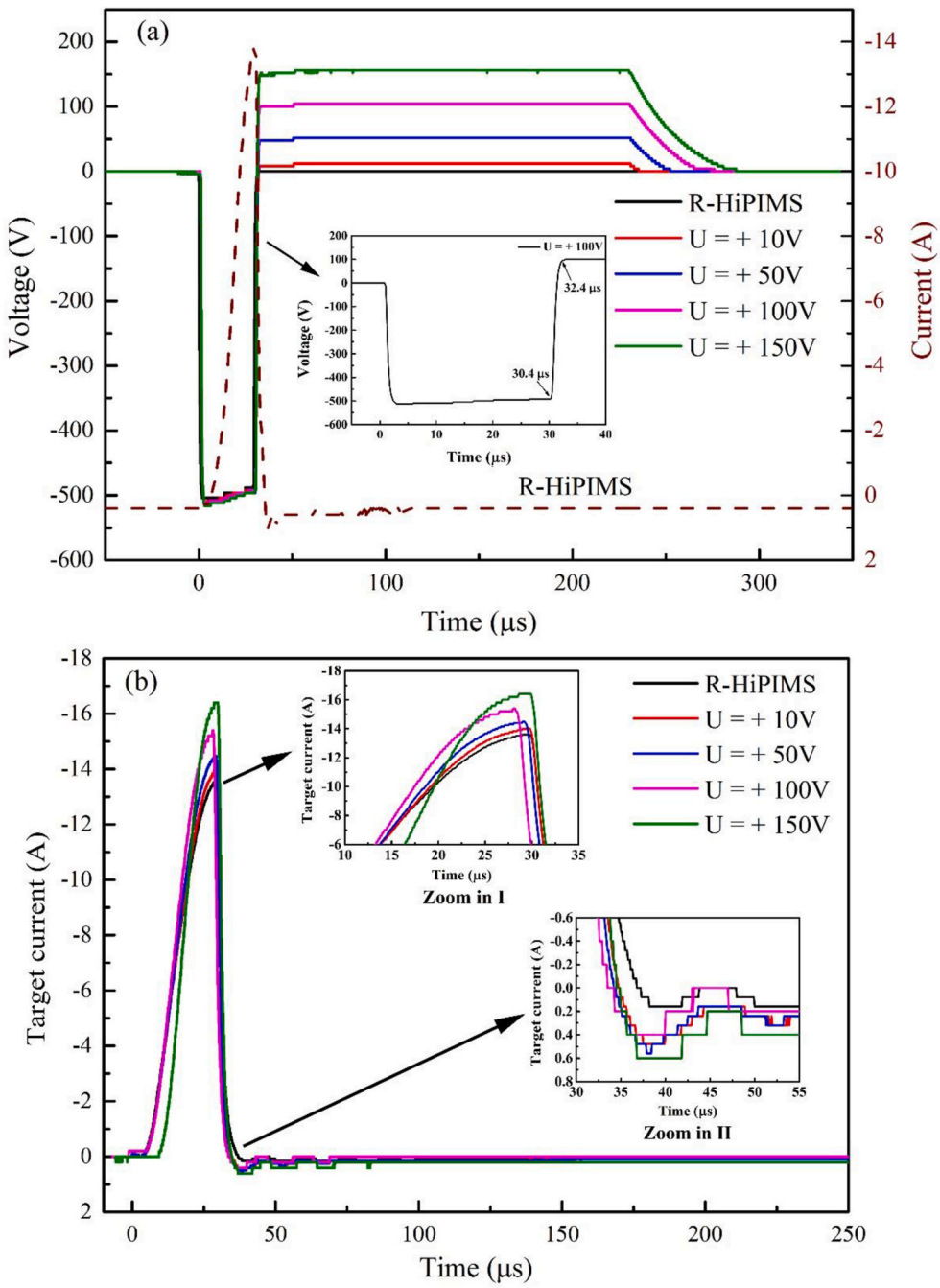

Fig. 7. HiPIMS discharge voltage (a) and current (b) waves with and without following extraction voltage pulses U ($U = 0$ V, 10 V, 50 V, 100 V or 150 V, $U = 0$ V is marked as R-HiPIMS).

I. For Ti^+, there was a narrow and sharp low-energy wave (within 4.5 eV) whose peak centered around 1.5–2.1 eV (Fig. 8(a)). The low-energy wave magnitude decreases gradually with increasing $U_{extract}$ while the peak position (energy) decreased from 2.1 eV (R-HiPIMS) to 1.5 eV ($U_{extract} = 70$ V) firstly and then increased to 1.7 eV ($U_{extract} = 150$ V) (Fig. 8(b)).

II. For Ti^+, a new equally-narrow and sharp wave appeared at the position of ion energy = 12.9 eV, 28.8 eV, 54 eV, 78.6 eV, for $U_{extract} = 10$ V, 25 V, 50 V, 75 V, respectively.

III. For Ti^+, to the right of this peak there was a shoulder and a long energy tail, similar to the standard HiPIMS [46]. The shoulder counts increased with the increase of the $U_{extract}$ especially notable as the $U_{extract} > 50$ V. Similar results also were reported in Ref. [48].

IV. For Ar^+, the Ar^+ energy distribution curves had similarities and differences as compared to the Ti^+ fluxes. There is also a narrow and sharp low-energy wave (below 4 eV) whose peak is centered at 1.2–1.5 eV. The low-energy wave also decreases gradually in counts with increasing $U_{extract}$ (Fig. 8(c) and (d)).

V. For Ar^+, there are also new equally-narrow and sharp waves at higher energy when applying the $U_{extract}$. However, new waves could be split into three sub-waves and were more notable for higher $U_{extract}$. The peak position was listed in Table 2. Unlike III (Ti^+), the shoulder to the right is not presented and the curve count descends quickly to the right especially for the R-HIPIMS, 10 V, and 25 V $U_{extract}$ cases. Similar results also were reported in Refs. [46,48]. For 50 V and 75 V cases, there was a slight rise in

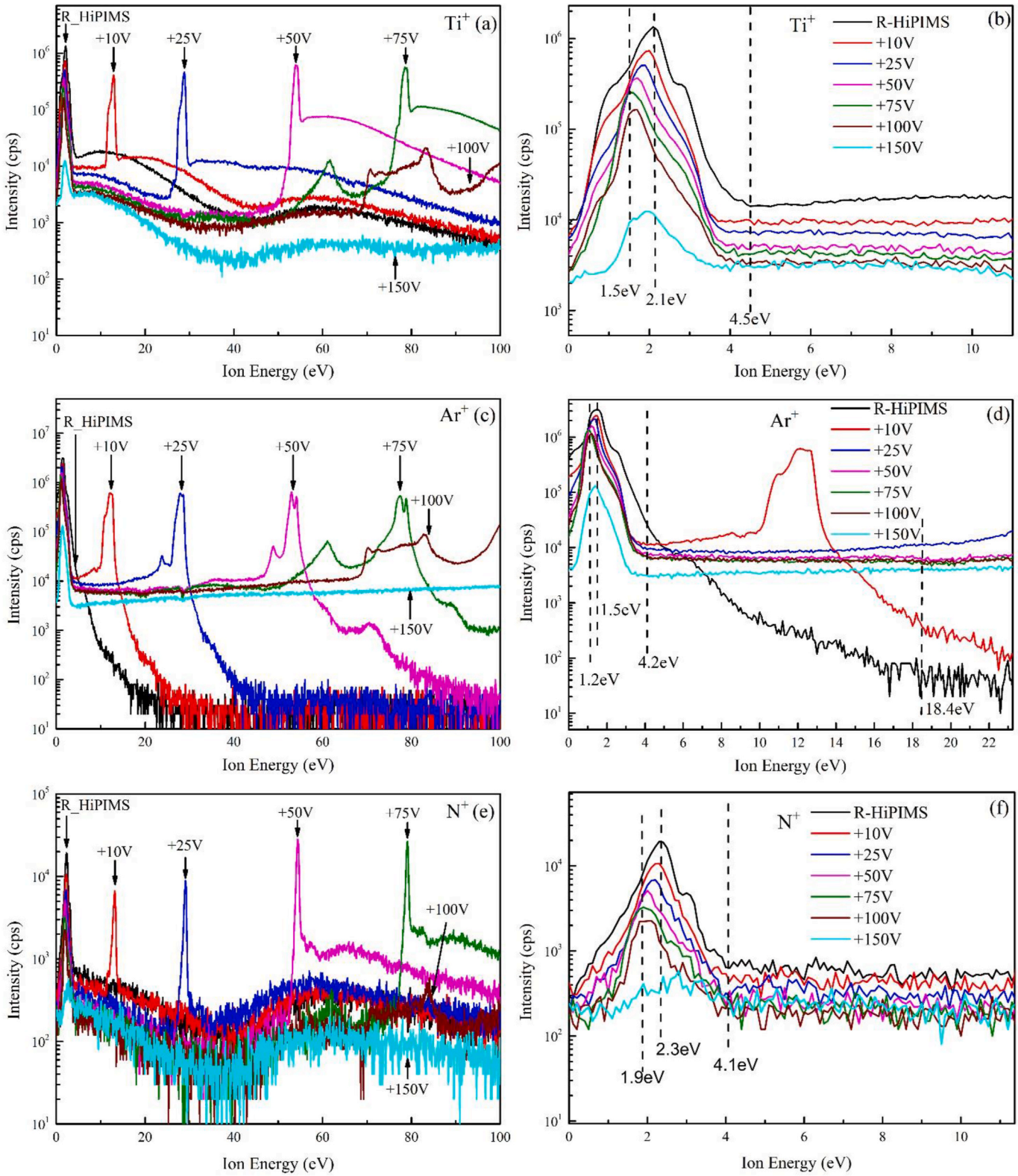

Fig. 8. The time-averaged ion energy distribution functions measured at the substrate position during bipolar HiPIMS sputtering of Ti in Ar/N_2.

Table 2
Peak position of split sub-waves of Ar^+.

Extraction voltage(V)	0	10			25			50			75		
Sub-waves abscissa position(eV)	–	11	12.1	12.6	23.8	28	28.6	48.9	53	54.1	61.2	77.5	78.8

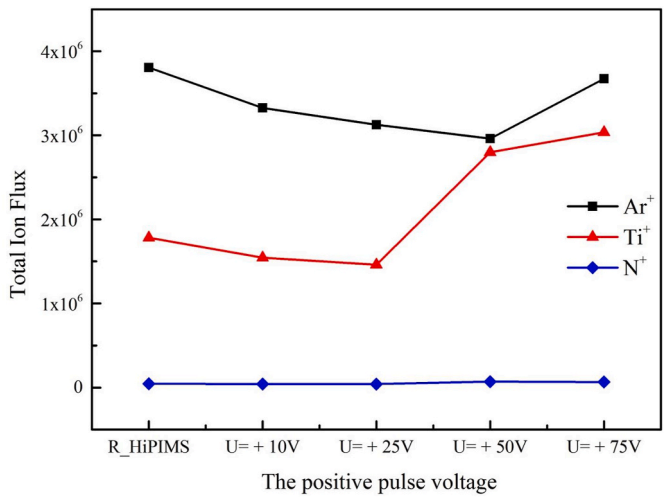

Fig. 9. The integrated intensities for Ar^+, Ti^+, N^+ ion flux curves.

higher energy, and another peak seems to appear at the higher energy position.

VI. For N^+, there There is also a narrow and sharp low-energy wave (within 4.1 eV) whose peak is centered around 1.9–2.3 eV (Fig. 8 (e) and (f)). The low-energy wave magnitude decreased gradually with increasing $U_{extract}$ while the peak position (energy) decreased from 2.3 eV (R-HiPIMS) to 1.9 eV ($U_{extract}$ = 75 V) firstly and then increased to 3 eV when $U_{extract}$ = 150 V (Fig. 8 (f)).

VII. For N^+, there are also new equally-narrow and sharp waves at higher energy when applying the $U_{extract}$. The new wave peak position was at 13.2 eV, 29.1 eV, 54.4 eV, 79.1 eV for $U_{extract}$ = 10 V, 25 V, 50 V, 75 V, respectively.

VIII. Whatever with or without the $U_{extract}$, there was a hump between 40 and 85 eV in any case, and when $U_{extract}$ = 75 V, a wave would appear whose peak position is at 61.7 eV, 61.2 eV, 61.8 eV for Ti^+, Ar^+, and N^+, respectively. If the $U_{extract}$ was applied, the intensity between the first sharp wave and the new wave would increase. This was conspicuous for Ar^+ because its right shoulder and high-energetic tail nearly disappeared.

The obtained IEDF waves characterized with a low-energy wave accompanied by a new higher energy wave were the direct evidence to show that the ions extraction method works. The formation of the high energy wave is due to the ions accelerated by the elevated plasma potential during the positive pulse [45,46], which is consistent with the simulation results of plasma potential (Figs. 4 and 6). To evaluate the ions extraction efficiency, Fig. 9 shows the integrated intensities of Ar^+, Ti^+, and, N^+ ion flux curves with an $U_{extract}$ of +10 V, 25 V, 50 V, and 75 V applied respectively. Because the ion mass spectrometer can only measure the ions with energies below 100 eV, so it is underestimated for the $U_{extract}$ = +50 V, +75 V cases. From Fig. 8, it can be reasonably deduced that there should also be a long tail to the right (>100 eV), the ions whose number of positive charges could be over 2, and the ions whose energy was over 100 eV were neglected. From Fig. 9, It can be seen that with a lower $U_{extract}$ of 10 V and 25 V, the ions total Ar^+ and Ti^+ fluxes even have a tendency to decrease, however, if the $U_{extract}$ reached to 50 V or more, the total Ti^+ and Ar^+ fluxes would increase. Especially for Ti^+ flux, though the ions with energy over 100 eV were not included, the Ti^+ ion flux dramatically increased when the $U_{extract}$ was over 50 V.

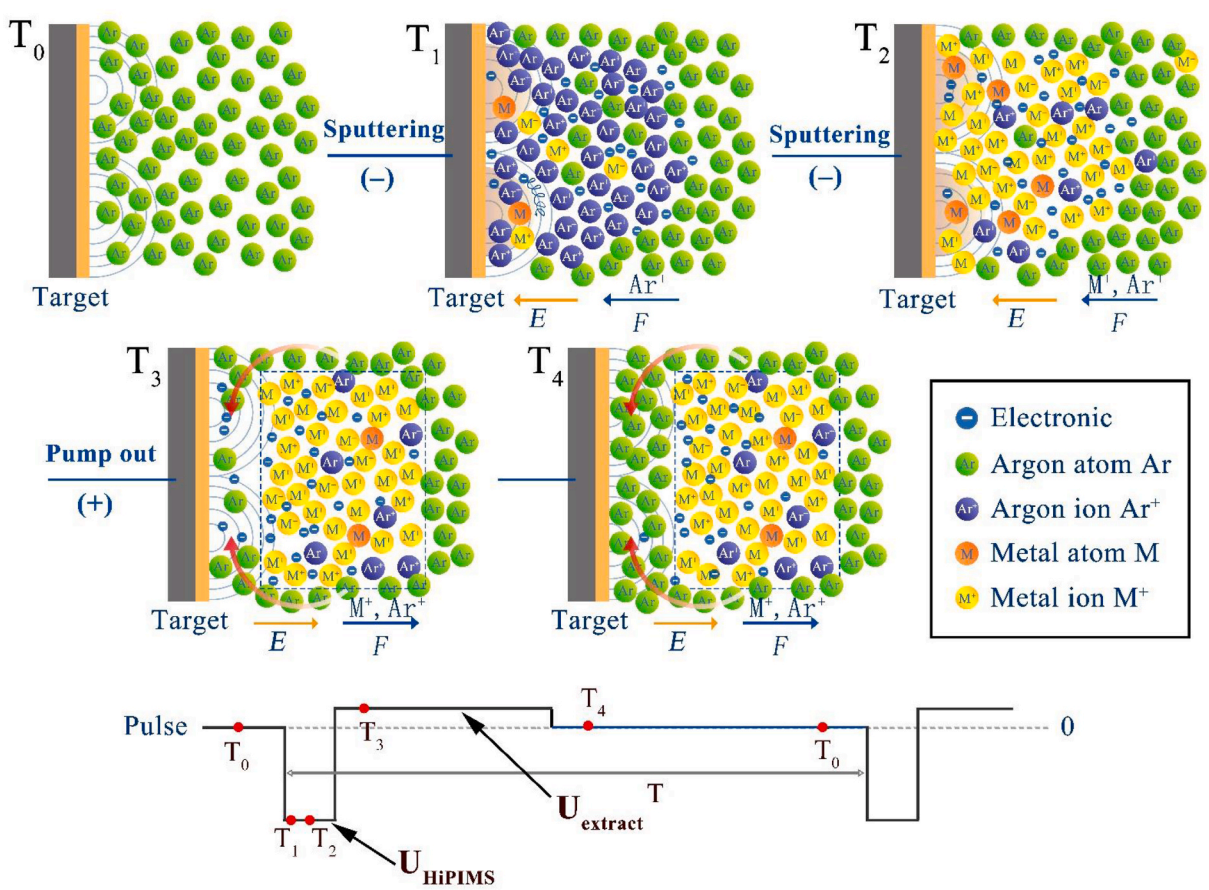

Fig. 10. Illustration of ions extraction mechanism.

That is the ions were successfully extracted out. At low positive pulse voltage, the reason for the decrease of the ion flux of Ar^+ and Ti^+ may be due to the plasma potential being higher than the vacuum furnace wall and the increase of ion diffusion to the chamber wall. At high positive pulse voltage, the reason for the increase of the ion flux of Ar^+ and Ti^+ may be due to the additional heating of electrons or reverse discharge [63–65], and the driving effect of the high electric field strength between the target and the substrate. The distribution and the peak position of ion density at different times in Fig. 5 is a piece of evidence. However, the increase of N ions and Ar ion flux has not the same tendency as that of Ti ions. By considering the simulation result of Fig. 5, a possible mechanism for this phenomenon, that is, the ions extraction mechanism is illustrated in Fig. 10.

In Fig. 10, at the time T_0, the target voltage was grounded. The HiPIMS discharge has not started. So there were Ar atoms in front of the target. At the time T_1, a high negative voltage U_{HiPIMS} was applied to the target. The glow discharge began at this time, and Ar^+ ions were created in front of the target and were attracted by the negative target. So the magnetron sputtering was triggered and the target metal atoms (Ti atoms in this case) were sputtered out. At the time of T_2, the metal self sputtering becomes dominated. The target metal ions (Ti ions in this case) were constantly increased, and these ions occupied the area in front of the target. The gas rarefaction becomes obvious, and the stationary sheath would be formed at this time. At the time T_3, the $U_{extract}$ was applied to the target, the electrons near the target are collected by the target and the ions were repelled. Because the mobility of ions was much less than that of the electrons, there should just be net charge particles which are the difference of positive ions number and electron number in front of the target. That is the reason why the simulation result shown in Fig. 4 indicated that there is a positive potential area higher than the positive pulse voltage $U_{extract}$. Just like the simulation result shown in Fig. 5, the ions would be repelled away from the target, which is the reason why the highest ions density area becomes farther and farther from the target. As the metal ions extracted out of the target surface area, the gas atom of Ar (as well as the N_2, not shown in Fig. 10) would be breathed in the target near the surface area. So the ions were extracted out, and the Ar gas was breathed in, alternatively. At the time T_4, if the $U_{extract}$ pulse width is not enough, the ions clouds (or plasma clouds) would drift to the substrate with the energy obtained by the $U_{extract}$. At a certain moment in the process from T_4 of the previous pulse to T_0 of the next pulse, the plasma will be extinguished and the chamber will return to the state at T_0. This is a continuous cycle.

5. Conclusion

This paper provides a method to extract out the ions from the ionization region of the HiPIMS by using a positive ions extraction pulse. The PIC-MCC simulation and experimental study were performed to explore the ions extraction procedure. The simulation results indicated that the higher potential and the peak ion density were gradually driven to the substrate direction, with the application of an ions extraction pulse to the target. Furthermore, the value of the peak ion density would continuously increase from 9.500×10^{16} m^{-3} to 3.430×10^{17} m^{-3}, when $U_{extract} = 400$ V. From the results of the experiment, the IEDF charactered with a low-energy wave accompanied by a new higher energy wave directly certificated that the ions extraction method works. When the $U_{extract}$ was over 50 V, the Ti^+ ions flux significantly increased. It can be concluded that the ions were successfully extracted out. Comparison between the simulation and experimental results showed a fairly good agreement. Based on the combination of simulative, experimental, and theoretical studies, the microscopic mechanism of ions extraction from the ionization region of the HiPIMS target was proposed finally.

CRediT authorship contribution statement

Liuhe Li: Writing – review & editing, Writing – original draft, Funding acquisition. **Jiabin Gu:** Writing – review & editing, Writing – original draft. **Yi Xu:** Writing – review & editing, Investigation. **Mingyue Han:** Writing – review & editing, Investigation. **Marcela Milena Marie Bilek:** Writing – review & editing, Investigation.

Declaration of competing interest

The authors declare that they have no known competing financial interests or personal relationships that could have appeared to influence the work reported in this paper.

Data availability

Data will be made available on request.

Acknowledgments

This work has been jointly supported by the National Science and Technology Major Project (No. 2017-VII-0012-0108) and National Defense Fundamental Research Project (No. JCKY2018601C205).

References

[1] A. Anders, A review comparing cathodic arcs and high power impulse magnetron sputtering (HiPIMS), Surf. Coating. Technol. 257 (2014) 308–325, https://doi.org/10.1016/j.surfcoat.2014.08.043.
[2] D. Lundin, M. Cada, Z. Hubicka, Ionization of sputtered Ti, Al, and C coupled with plasma characterization in HiPIMS, Plasma Sources Sci. Technol. 24 (2015), 035018, https://doi.org/10.1016/j.vacuum.2018.01.039.
[3] V. Kouznetsov, K. Macak, J.M. Schneider, U. Helmersson, I. Petrov, A novel pulsed magnetron sputter technique utilizing very high target power densities, Surf. Coating. Technol. 122 (1999) 290–293, https://doi.org/10.1016/S0257-8972(99)00292-3.
[4] K. Macák, V. Kouznetsov, J. Schneider, U. Helmersson, I. Petrov, Ionized sputter deposition using an extremely high plasma density pulsed magnetron discharge, J. Vac. Sci. Technol. A, Vac. Surf. Films 18 (2000) 1533–1537, https://doi.org/10.1116/1.582380.
[5] A.P. Ehiasarian, W.-D. Münz, L. Hultman, U. Helmersson, I. Petrov, High power impulse magnetronsputtered CrN_x films, Surf. Coating. Technol. 163–164 (2003) 267–272, https://doi.org/10.1016/S0257-8972(02)00479-6.
[6] J.T. Gudmundsson, J. Alami, U. Helmersson, Evolution of the electron energy distribution and the plasma parameters in a pulsed magnetron discharge, Appl. Phys. Lett. 78 (22) (2001) 3427–3429, https://doi.org/10.1063/1.1376150.
[7] A.P. Ehiasarian, R. New, W.D. Munz, L. Hultman, U. Helmersson, V. Kouznetsov, Influence of high power densities on the composition of pulsed magnetron plasmas, Vacuum 65 (2002) 147–154, https://doi.org/10.1016/S0042-207X(01)00475-4.
[8] J. Bohlmark, J.T. Gudmundsson, J. Alami, M. Lattemann, U. Helmersson, Spatial electron density distribution in a high-power pulsed magnetron discharge, IEEE Tras. Plasma Sci. 33 (2005) 346–347, https://doi.org/10.1109/TPS.2005.845022.
[9] J. Alami, J.T. Gudmundsson, J. Bohlmark, J. Birch, U. Helmersson, Plasma dynamics in a highly ionized pulsed magnetron discharge, Plasma Sources Sci. Technol. 14 (2005) 525–531, https://doi.org/10.1088/0963-0252/14/3/015.
[10] J. Bohlmark, M. Lattemann, J.T. Gudmundsson, A.P. Ehiasarian, Y. Aranda Gonzalvo, N. Brenning, U. Helmersson, The ion energy distributions and ion flux composition from a high power impulse magnetron sputtering discharge, Thin Solid Films 515 (2006) 1522, https://doi.org/10.1016/j.tsf.2006.04.051.
[11] A.P. Ehiasarian, Y.A. Gonzalvo, T.D. Whitmore, Time-resolved ionisation studies of the high power impulse magnetron discharge in mixed argon and nitrogen atmosphere, Plasma Process. Polym. 4 (2007) S309–S313, https://doi.org/10.1002/ppap.200730806.
[12] D.J. Christie, Target material pathways model for High power impulse magnetron sputtering, J. Vac. Sci. Technol. A, Vac. Surf. Films 23 (2005) 330–335, https://doi.org/10.1116/1.1865133.
[13] U. Helmersson, M. Lattemann, J. Bohlmark, A.P. Ehiasarian, J.T. Gudmundsson, Ionized physical vapor deposition (IPVD): a review of technology and applications, Thin Solid Films 513 (2006) 1–24, https://doi.org/10.1016/j.tsf.2006.03.033.
[14] J. Emmerlich, S. Mraz, R. Snyders, K. Jiang, J.M. Schneider, The physical reason for the apparently low deposition rate during high-power pulsed magnetron sputtering, Vacuum 82 (2008) 867–870, https://doi.org/10.1016/j.vacuum.2007.10.011.
[15] U. Helmersson, M. Lattemann, J. Alami, J. Bohlmark, A.P. Ehiasarian, J. T. Gudmundsson, High power impulse magnetron sputtering discharges and thin film growth: a brief review, in: Proceedings of 48th Annual Technical Conferenece Proceedings of the Society of Vacuum Coaters. Denver, CO, 2005, pp. 458–464.

[16] J.A. Davis, W.D. Sproul, D.J. Christie, M. Geisler, High power pulse reactive sputtering of TiO_2, in: Proceedings of 47th Annual Technical Conferenece Proceedings of the Society of Vacuum Coaters. Dallas, TX, 2004, pp. 215–218.

[17] Q. Ma, L. Li, Y. Xu, J. Gu, L. Wang, Y. Xu, Effect of bias voltage on TiAlSiN nanocomposite coatings deposited by HiPIMS, Appl. Surf. Sci. 392 (2017) 826–833, https://doi.org/10.1016/j.apsusc.2016.09.028.

[18] R. Ganesan, B. Treverrow, P. Denniss, D.G. McCulloch, D.R. McKenzie, M.M. M. Bilek, Pulsed external magnetic fields increase the deposition rate in reactive HiPIMS while preserving stoichiometry: an application to amorphous HfO_2, J. Appl. Phys. 120 (10) (2016), 103301, https://doi.org/10.1063/1.4961730.

[19] D.J. Christie, Target material pathways model for High power impulse magnetron sputtering, J. Vac. Sci. Technol., A 23 (2005) 330. https://doi:10.1116/1.1865133.

[20] N. Brenning, C. Huo, D. Lundin, M.A. Raadu, C. Vitelaru, G.D. Stancu, T. Minea, U. Helmersson, Understanding deposition rate loss in high power impulse magnetron sputtering: I. Ionization-driven electric fields, Plasma Sources Sci. Technol. 21 (2) (2012), 025005. https://doi:10.1088/0963-0252/21/2/025005.

[21] N. Britun, M. Palmucci, S. Konstantinidis, R. Snyders, Particle visualization in high-power impulse magnetron sputtering. I. 2D density mapping, J. Appl. Phys. 117 (16) (2015), 163302, https://doi.org/10.1063/1.4919006.

[22] R. Chistyakov, B. Abraham, W.D. Sproul, Advances in high power pulse reactive magnetron sputtering, in: Proceedings of the 49th Annual SVC Technical Conference, Washington, DC, April 23-27 2006, pp. 88–91.

[23] R. Chistyakov, B. Abraham, W. Sproul, J. Moore, J. Lin, Modulated pulse power technology and deposition for protective and tribological coatings, in: Proceedings of the 50th Annual SVC Technical Conference, Louisville, KY, 2007, pp. 139–143.

[24] J. Lin, W.D. Sproul, J.J. Moore, Z.L. Wu, S. Lee, R. Chistyakov, B. Abraham, Recent advances in modulated pulsed power magnetron sputtering for surface engineering, JOM-US 63 (6) (2011) 48–58.

[25] J. Lin, W.D. Sproul, J.J. Moore, in: Influence of the Magnetic Field Strength on the Deposition Rate of Modulated Pulsed Power (MPP) Magnetron Sputtering of Metallic Thin Films Proceedings of the AVS 57th International Symposium & Exhibition, Albuquerque, New Mexico, 2010.

[26] J. Lin, J.J. Moore, W.D. Sproul, S.L. Lee, Effects of the magnetic field strength on the modulated pulsed power magnetron sputtering of metallic films, J. Vac. Sci. Technol., A 29 (2011), 061301, https://doi.org/10.1116/1.3645612.

[27] P. Vašina, M. Meško, L. de Poucques, J. Bretagne, C. Boisse-Laporte, M. Touzeau, Study of a fast High power impulse magnetrondischarge: role of plasma deconfinement on the charged particle transport, Plasma Sources Sci. Technol. 17 (2008), 035007, https://doi.org/10.1088/0963-0252/17/3/035007.

[28] X. Zuo, R. Chen, J. Liu, P. Ke, A. Wang, The influence of superimposed DC current on electrical and spectroscopic characteristics of HiPIMS discharge, AIP Adv. 8 (2018), 015132, https://doi.org/10.1063/1.5018037.

[29] J. Olejnicek, Z. Hubicka, S. Kment, M. Cada, P. Ksirova, P. Adamek, I. Gregora, Investigation of reactive HiPIMS + MF sputtering of TiO_2 crystalline thin films, Surf. Coat. Technol. 232 (2013) 376–383, https://doi.org/10.1016/j.surfcoat.2013.05.038.

[30] V.O. Oskirko, A.N. Zakharov, A.P. Pavlov, A.A. Solovyev, V.A. Semenov, S. V. Rabotkin, Hybrid HIPIMS+ MFMS power supply for dual magnetron sputtering systems, Vacuum 181 (2020), 109670, https://doi.org/10.1016/j.vacuum.2020.109670.

[31] M. Lattemann, B. Abendroth, A. Moafi, D.G. McCulloch, D.R. McKenzie, Controlled glow to arc transition in sputtering for high rate deposition of carbon films, Diam. Relat. Mater. 20 (2011) 68–74, https://doi.org/10.1016/j.diamond.2010.11.007.

[32] A. Mishra, P.J. Kelly, J.W. Bradley, The evolution of the plasma potential in a HiPIMS discharge and its relationship to deposition rate, Plasma Sources Sci. Technol. 19 (2010), 045014, https://doi.org/10.1088/0963-0252/19/4/045014.

[33] J. Čapek, M. Hála, O. Zabeida, J.E. Klemberg-Sapieha, L. Martinu, Deposition rate enhancement in HiPIMS without compromising the ionized fraction of the deposition flux, J. Phys. D Appl. Phys. 46 (2013), 205205, https://doi.org/10.1088/0022-3727/46/20/205205.

[34] H. Hajihoseini, J.T. Gudmundsson, Vanadium and vanadium nitride thin films grown by high power impulse magnetron sputtering, J. Phys. D Appl. Phys. 50 (50) (2017), 505302, https://doi.org/10.1088/1361-6463/aa96f2.

[35] J. McLain, P. Raman, D. Patel, R. Spreadbury, J. Uhlig, I. Shchelkanov, D.N. Ruzic, Linear magnetron HiPIMS high deposition rate magnet pack, Vacuum 155 (2018) 559–565, https://doi.org/10.1016/j.vacuum.2018.06.023.

[36] C. Li, X. Tian, C. Gong, S. Liu, Electric and magnetic fields synergistically enhancing high power impulse magnetron sputtering deposition of vanadium coatings, Vacuum 144 (2017) 125–134, https://doi.org/10.1016/j.vacuum.2017.07.032.

[37] S. Konstantinidis, J.P. Dauchot, M. Ganciu, A. Ricard, M. Hecq, Influence of pulse duration on the plasma characteristics in high-power pulsed magnetron discharges, J. Appl. Phys. 99 (2006), 013307, https://doi.org/10.1063/1.2159555.

[38] T.T. Nakano, C. Murata, S. Baba, Effect of the target bias voltage during off-pulse period on the impulse magnetron sputtering, Vacuum 84 (12) (2010) 1368–1371, https://doi.org/10.1016/j.vacuum.2010.01.014.

[39] M. Han, Y. Luo, L. Li, J. Gu, Y. Xu, S. Luo, Optimizing the ion diffusion in bipolar-pulse HiPIMS discharge (BP-HiPIMS) via an auxiliary anode, Plasma Sources Sci. Technol. 30 (9) (2021), 095016, https://doi.org/10.1088/1361-6595/ac1383.

[40] L. Li, A New Method of Pumping Ions from Solid Metal and Research on Several Related Scientific Issues *the*, National Science Foundation of China, 2016 (*Declined*).

[41] M. Han, Y. Luo, L. Tang, J. Gu, H. Li, Y. Xu, S. Luo, L. Li, Plasma flux and energy enhancement in BP-HiPIMS discharge via auxiliary anode and solenoidal coil, Plasma Sources Sci. Technol. 30 (11) (2021), 115002, https://doi.org/10.1088/1361-6595/ac2c8c.

[42] T. Nakano, N. Hirukawa, S. Saeki, S. Baba, Effects of target voltage during pulse-off period in pulsed magnetron sputtering on afterglow plasma and deposited film structure, Vacuum 87 (2013) 109–113, https://doi.org/10.1016/j.vacuum.2012.03.010.

[43] B. Wu, I. Haehnlein, I. Shchelkanov, J. McLain, D. Patel, J. Uhlig, B. Jurczyk, Y. Leng, D.N. Ruzic, Cu films prepared by bipolar pulsed high power impulse magnetron sputtering, Vacuum 150 (2018) 216–221, https://doi.org/10.1016/j.vacuum.2018.01.011.

[44] N. Britun, M. Michiels, T. Godfroid, R. Snyders, Ion density evolution in a high-power sputtering discharge with bipolar pulsing, Appl. Phys. Lett. 112 (2018), 234103, https://doi.org/10.1063/1.5030697.

[45] V. Tiron, I.-L. Velicu, Understanding the ion acceleration mechanism in bipolar HiPIMS: the role of the double layer structure developed in the after-glow plasma, Plasma Sources Sci. Technol. 29 (2020), 015003, https://doi.org/10.1088/1361-6595/ab6156.

[46] J. Keraudy, R.P.B. Viloan, M.A. Raadu, N. Brenning, D. Lundin, U. Helmersson, Bipolar HiPIMS for tailoring ion energies in thin film deposition, Surf. Coat. Technol. 359 (2019) 433–437, https://doi.org/10.1016/j.surfcoat.2018.12.090.

[47] R.P.B. Viloan, M. Zaňáška, D. Lundin, U. Helmersson, Pulse length selection for optimizing the accelerated ion flux fraction of a bipolar HiPIMS discharge, Plasma Sources Sci. Technol. 29 (2020), 125013, https://doi.org/10.1088/1361-6595/abc6f6.

[48] R. Hippler, M. Cada, Z. Hubicka, Time-resolved Langmuir probe diagnostics of a bipolar high power impulse magnetron sputtering discharge, Appl. Phys. Lett. 116 (2020), 064101, https://doi.org/10.1063/1.5140650.

[49] R.P.B. Viloan, J. Gu, R. Boyd, J. Keraudy, L. Li, U. Helmersson, Bipolar high power impulse magnetron sputtering for energetic ion bombardment during TiN thin film growth without the use of a substrate bias, Thin Solid Films 688 (2019), 137350, https://doi.org/10.1016/j.tsf.2019.05.069.

[50] R. Hippler, M. Cada, Z. Hubicka, Direct current and high power impulse magnetron sputtering discharges with a positively biased anode, J. Vac. Sci. Technol., A 39 (4) (2021), 043007, https://doi.org/10.1116/6.0001054.

[51] Š. Batková, J. Čapek, J. Rezek, R. Čerstvý, P. Zeman, Effect of positive pulse voltage in bipolar reactive HiPIMS on crystal structure, microstructure and mechanical properties of CrN films, Surf. Coat. Technol. 393 (2020), 125773, https://doi.org/10.1016/j.surfcoat.2020.125773.

[52] V. Tiron, E.-L. Ursu, D. Cristea, D. Munteanu, G. Bulai, A. Ceban, I.-L. Velicu, Overcoming the insulating materials limitation in HiPIMS: ion-assisted deposition of DLC coatings using bipolar HiPIMS, Appl. Surf. Sci. 494 (2019) 871–879, https://doi.org/10.1016/j.apsusc.2019.07.239.

[53] D.T. Kwok, C. Cornet, Numerical simulation of metal plasma immersion ion implantation (MePIIID) on a sharp cone and a fine tip by a multiple-grid particle-in-cell (PIC) method, IEEE Trans. Plasma Sci. 34 (2006) 2434–2442, https://doi.org/10.1109/TPS.2006.883366.

[54] C. Cornet, D.T.K. Kwok, A new algorithm for charge deposition for multiple-grid method for PIC simulations in r-z cylindrical coordinates, J. Comput. Phys. 225 (1) (2007) 808–828, https://doi.org/10.1016/j.jcp.2007.01.004.

[55] J. Luo, Theoretical and Applied Research of Enhanced Glow Discharge Plasma Immersion Ion Implantation and Deposition, Ph.D Thesis, Beihang University, 2014 (in Chinese).

[56] V. Vahedi, M. Surendra, A Monte Carlo collision model for the particle-in-cell method: applications to argon and oxygen discharges, Comput. Phys. Commun. 87 (1–2) (1995) 179–198, https://doi.org/10.1016/0010-4655(94)00171-W.

[57] W. En, N.W. Cheung, A new method for determining the secondary electron yield dependence on ion energy for plasma exposed surfaces, IEEE Trans. Plasma Sci. 24 (1996) 1184–1187, https://doi.org/10.1109/27.533128.

[58] P. Poolcharuansin, J. Bradley, Short-and long-term plasma phenomena in a HiPIMS discharge, Plasma Sources Sci. Technol. 19 (2) (2010), 025010, https://doi.org/10.1088/0963-0252/19/2/025010.

[59] A. Revel, T. Minea, C. Costin, 2D PIC-MCC simulations of magnetron plasma in HiPIMS regime with external circuit, Plasma Sources Sci. Technol. 27 (2018), 105009, https://doi.org/10.1088/1361-6595/aadebe.

[60] T.M. Minea, C. Costin, A. Revel, D. Lundin, L. Caillault, Kinetics of plasma species and their ionization in short-HiPIMS by particle modeling, Surf. Coating. Technol. 255 (2014) 52–61, https://doi.org/10.1016/j.surfcoat.2013.11.050.

[61] J.H. In, B.K. Na, S.H. Seo, H.Y. Chang, J.G. Han, Three-step decay of the plasma density near the substrate in pulsed-dc magnetron sputtering discharge, Plasma Sources Sci. Technol. 18 (2009), 045029, https://doi.org/10.1088/0963-0252/18/4/045029.

[62] I.-L. Velicu, G.-T. Ianoş, C. Porosnicu, I. Mihăilă, I. Burducea, A. Velea, D. Cristea, D. Munteanu, V. Tiron, Energy-enhanced deposition of copper thin films by bipolar high power impulse magnetron sputtering, Surf. Coat. Technol. 359 (2019) 97–107, https://doi.org/10.1016/j.surfcoat.2018.12.079.

[63] R. Hippler, M. Cada, Z. Hubicka, Time-resolved diagnostics of a bipolar HiPIMS discharge, J. Appl. Phys. 127 (2020), 203303, https://doi.org/10.1063/5.0006425.

[64] R. Hippler, M. Cada, V. Stranak, Z. Hubicka, Time-resolved optical emission spectroscopy of a unipolar and a bipolar pulsed magnetron sputtering discharge in an argon/oxygen gas mixture with a cobalt target, Plasma Sources Sci. Technol. 28 (2019), 115020, https://doi.org/10.1088/1361-6595/ab54e8.

[65] M.A. Law, F.L. Estrin, M.D. Bowden, J.W. Bradley, Diagnosing asymmetric bipolar HiPIMS discharges using laser Thomson scattering, Plasma Sources Sci. Technol. 30 (10) (2021), 105019, https://doi.org/10.1088/1361-6595/ac2be4.